

Development of a real-fluid based OpenFOAM solver for transcritical and supercritical flows

Danh Nam Nguyen, Jae Hun Lee, Chun Sang Yoo

Department of Mechanical Engineering, Ulsan National Institute of Science and Technology
Ulsan, Republic of Korea

1 Introduction

Recently a lot of research effort is put into the understanding and investigation of the injection and combustion processes under engine-relevant conditions (i.e., rocket engines or gas turbine engines) where high operating pressure is adopted for higher thermal efficiency. In that context, OpenFOAM (OF) as computational fluid dynamics (CFD) has become an indispensable tool for the investigation of such processes. However, official versions of the OF are not able to simulate nonreacting/reacting flows under transcritical and supercritical conditions because they require not only real-fluid models but also a robust solver that can numerically handle the highly non-linear behaviors of the fluid [2]. Some of the most widely used real-fluid models such as modified Soave-RedlichKwong (SRK) [3,4]/Peng-Robinson (PR) [5] equation of state models, Chung's model [6] for transport properties developed in OF-6 by Nguyen et al. [2] have been available for public use. Although a few OF-based solvers have been developed by several groups [7-10] for turbulent simulations under transcritical and supercritical conditions using real-fluid models, their source code are only available for limited people in their groups.

This work aims to complete our previous studies [2] providing for public use a robust OF-based platform for simulations of nonreacting/reacting flows at high pressure conditions accounting for real-fluid effects using RANS/LES methods. To this end, we develop a new solver for turbulent flow simulations under transcritical and supercritical conditions based on the official *reactingFoam* solver [1] and the available real-fluid *thermophysicalModel* library [2]. The developed solver is then validated against experimental data and previous studies by performing LES of cryogenic nitrogen jet flows. This work also intentionally provides a better understanding of the development of a modified pressure-based solution algorithm [7,9] in OF using real-fluid models.

2 Governing equations and solution algorithms

reactingFoam is modified as a basis to develop the new solver. Its governing equations including conservations of mass, momentum, species, and energy are given as:

$$\frac{\partial \rho}{\partial t} + \nabla \cdot (\rho \mathbf{U}) = 0 \quad (1)$$

$$\frac{\partial(\rho \mathbf{U})}{\partial t} + \nabla \cdot (\rho \mathbf{U} \mathbf{U}) = -\nabla p + \nabla \cdot \boldsymbol{\tau} \quad (2)$$

$$\frac{\partial \rho Y_i}{\partial t} + \nabla \cdot (\rho \mathbf{U} Y_i) = \nabla \cdot (\mu_{eff} \nabla Y_i) + \dot{w}_i \quad (3)$$

$$\frac{\partial (\rho h_s)}{\partial t} + \nabla \cdot (\rho \mathbf{U} h_s) + \frac{\partial (\rho K)}{\partial t} + \nabla \cdot (\rho \mathbf{U} K) = \frac{\partial p}{\partial t} + \nabla \cdot (\alpha_{eff} \nabla h) + \dot{Q} \quad (4)$$

where t is the time, ρ the density of mixture, \mathbf{U} the velocity vector, p the pressure, $\boldsymbol{\tau}$ viscous stress tensor, h_s the sensible enthalpy, K the kinematic energy, \dot{Q} the heat of combustion, Y_i and \dot{w}_i , are the mass fraction and the production rate of i -th species. μ_{eff} and α_{eff} are effective viscosity and effective thermal diffusivity, respectively. These quantities consist of a laminar and turbulent part (i.e., $\mu_{eff} = \mu + \mu_t$ and $\alpha_{eff} = \alpha + \alpha_t$). It is important to note that all laminar thermophysical properties are evaluated using real-fluid models as described in [2], while turbulent parts are calculated based on turbulent models selected by a user on runtime. The above governing equations can be applied to both RANS and LES approaches, in which some simplified assumptions have been made. For instance, unity Schmidt and Lewis numbers are adopted; mass diffusion fluxes are closed with the Fick's law; and the Dufour effect, Soret effect and radiative heat transfer are neglected.

To improve the stability of the solution algorithm for the numerical simulations using real-fluid models, a special pressure-based solution method proposed by Jarczyk et al. [7] is adopted. In this method, there are two crucial changes for real-fluid problems compared to ideal gas ones. First, the pressure equation needs to be modified to account for the real-fluid effects due to the dependence of the compressibility on pressure as shown in Eq. 5. Second, the procedure in the PISO (Pressure Implicit with Splitting of Operators) loop must also be adapted. The details can be found in [7,9].

$$\underbrace{\frac{\partial (\rho^{n-1} \Psi^{n-1} p^{n-1})}{\partial t}}_{\text{explicit}} + \underbrace{\frac{\partial \Psi^{n-1} p}{\partial t}}_{\text{implicit}} + \nabla \cdot \left[\rho \left(\frac{H_p}{a_p} \right) \right] - \nabla \cdot \left(\frac{\rho}{a_p} \nabla p \right) = 0 \quad (5)$$

where Ψ is the compressibility, P is the index of respective cell, a_p represents the diagonal coefficients of the matrix of a semi-discrete form of the momentum equation and H_p contains all off-diagonal contributions and the source term. The superscript $n - 1$ denotes the last time or iteration step [9]. To provide a better understanding of its implementation, the detailed code of the pressure equation is shown in Fig. 1. It can be seen from the figure that two first terms are added for the real-fluid problems compared to that of for ideal gas. In these terms, definitions of *rho* and *psi* are same as in the original *reactingFoam*.

```
fvScalarMatrix pEqn
(
    fvc::ddt(rho) //for real-fluid
    - fvc::ddt(psi, p) //for real-fluid
    + fvm::ddt(psi, p)
    + fvc::div(phiHbyA)
    - fvm::laplacian(rhoAUf, p)
    ==
    fvOptions(psi, p, rho.name())
);
```

Figure 1: The implementation of pressure equation for real-fluid problems in OpenFOAM.

It is worth mentioning that the sensible enthalpy is utilized as primary variable instead of the temperature in the energy equation. Therefore, the temperature is retrieved after solving the energy and species equations. This is done by using the iterative Newton's method for ideal gas problems as shown in Fig. 2-a. However, it does not always guarantee the convergence of the solution for real-fluid cases especially under transcritical conditions due to the pseudo-boiling phenomena. Recently there is no clear explanation in the literature for solutions to the problem applied in OF. In this work, we adopt a fast and robust coupling Newton-Bisection method motivated from the work of Hickey et al. [11] for a density-based solver as shown in Fig. 2-b to overcome that problem. In this method, first the Newton's approach

is employed (for speed). If the convergence is not achieved after 50 iterations, the algorithm is re-initialized, and the bisection method is adopted for robustness. Moreover, the derivative of the enthalpy with respect to temperature is also adapted to account for real-fluid effects (i.e., $dh/dT = C_{p,id} + df/dT$ where f is the departure function taken from the real-fluid equation of state model). The detailed derivation of this term is not presented here for the sake of brevity.

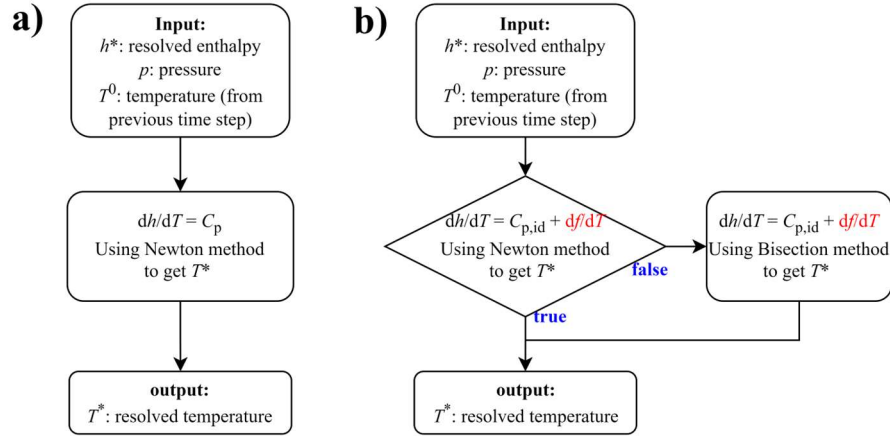


Figure 2: The algorithm to retrieve the temperature from the transported sensible enthalpy in OpenFOAM: a) for ideal gas; b) for real-fluid problem.

3 Validations and discussions

The turbulent jet mixing processes of a cryogenic liquid nitrogen (LN₂) injected into a quiescent gaseous nitrogen (GN₂) environment which are conducted experimentally by Mayer and coworkers [12] (i.e., Case 3 and Case 4) are examined using LES approach under transcritical and supercritical conditions to validate the developed solver. Detailed descriptions of these cases can be found in [12] while the boundary conditions are summarized in table 1. From a modeling point of view, Case 3 having the injection temperature lower than the pseudo-boiling temperature ($T_{pb}=129.53$ K) is the most interesting due to the regime of large density gradients [8]. As shown in Fig. 3, the density of the injected LN₂ in Case 3 is much higher than in Case 4.

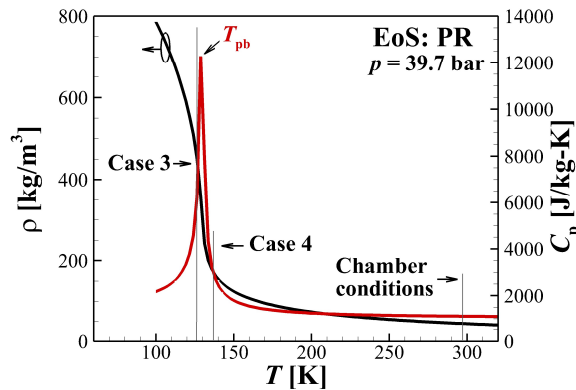


Figure 3: The thermodynamic properties of LN₂ and GN₂ for Case 3 and Case 4 produced by the PR equation of state model [5].

Table 1: Initial and boundary conditions [8,12]

Investigated cases	Chamber pressure [MPa]	Chamber temperature [K]	Injection temperature [K]	Injection velocity [m/s]
Case 3	3.97	298	126.9	4.9
Case 4	3.98	298	137.0	5.4

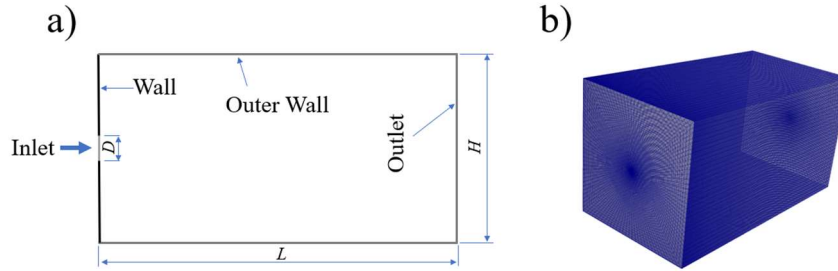


Figure 4: The configuration (a) and the computational domain (b) of the cryogenic nitrogen jet flows.

Figure 4 illustrates the configuration and the computational domain of validation cases. The computational domain includes the injector with a diameter of $D = 2.2$ mm. Its outer dimensions are $H \times H \times L = 60 \times 60 \times 80$ mm³ consisting of approximately 4.2 million cells. This number of grids is sufficient to resolve the flow, consistent with [8].

Different real-fluid models available in the real-fluid *thermophysicalModels* library [2] can be used in the developed solver. However, only PR equation of state [5] and Chung’s model [6] for transport properties are adopted in the present study for demonstration purpose. LES method with Smagorinsky model [13] is utilized. All simulations are performed using second-order schemes for both spatial discretization and time integration.

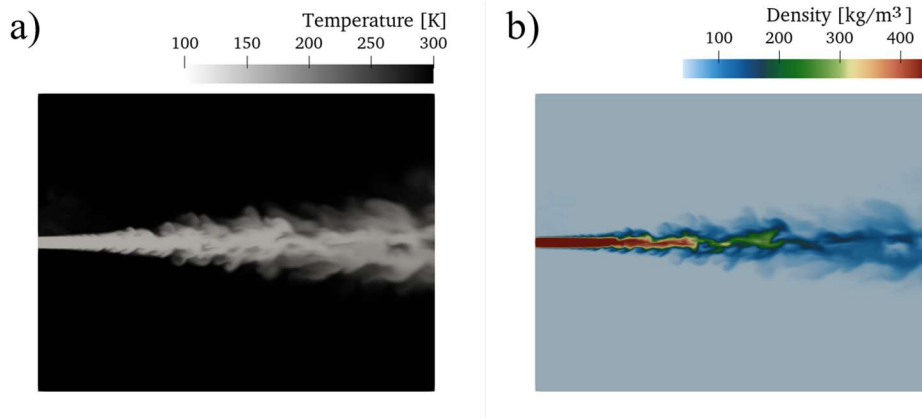


Figure 5: The instantaneous distribution of the temperature (a) and the density (b) of the cryogenic nitrogen jet flow in Case 3.

Figure 5 shows snapshots of the temperature and density distribution in Case 3. It can be observed that a very sharp, non-disturbed jet boundary occurs right after the injector exit and there is a large density difference between the core and the surrounding. This hinders the formation of Kelvin-Helmholtz vortices leading to a delay of jet breakup [8]. Since the temperature of the nitrogen injected into the chamber is lower than pseudo-boiling temperature, there is a layer of high heat capacity at the shear

layer between warm and cold nitrogen (not shown here), which implies that it needs higher energy to obtain a certain temperature increment at the surface of the cryogenic core. As a result, heat transfer from the warm surrounding is hindered by the large density stratification at the shear layer.

For quantitative assessment, Fig. 6 shows the time-averaged density profiles of Cases 3 and 4 along the centerline obtained by the present work compared to experimental data [12]. The results are also compared with the numerical results of Muller et al. [8] as a reference. As can be seen cases are reproduced in satisfactory agreement with the experiments from Mayer et al. [12]. Particularly, the simulation for Case 4 (supercritical) matches the benchmark data considerably well while that for Case 3 (transcritical) is not fully captured due to inconsistency of the injection temperature in the experiments [8]. The predicted data are also identical with the solution obtained from Muller et al. [8] as shown in Fig. 6-a. This implies that our implementation is proper, and the developed solver can be used for simulations of transcritical and supercritical flows.

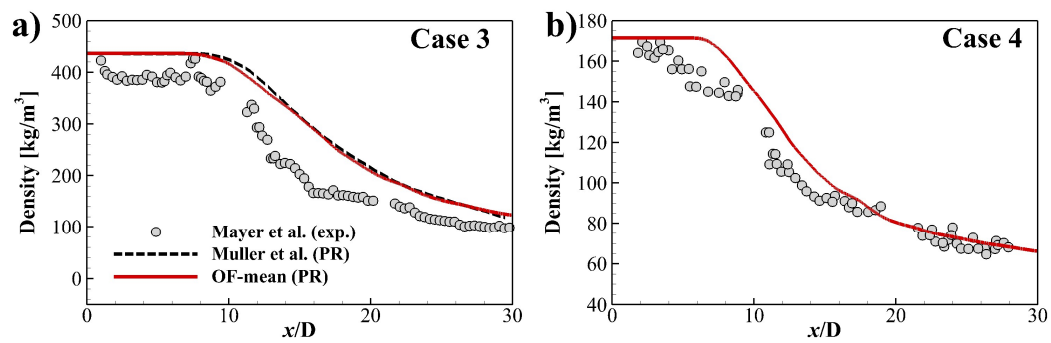


Figure 6: The profile of mean density along the centerline for Case 3 (a) and Case 4 (b) obtained from the present study (red lines) compared with experimental data (symbols) from Mayer et al. [12] and numerical solutions (black dash-lines) obtained by the work of Muller and coworkers [8].

For the computation, 96 cores of an Intel Xeon(R) Platinum 9242 2.3GHz processor are used for simulations. The wall clock time for Case 3 is 170 h corresponding to 16,336 CPU-hr while that of Case 4 is 87 h (8,315 CPU-hr). This is because Case 3 needs more iterations (i.e., more computational time) than Case 4 to handle the highly non-linear behaviors of the fluid due to its injection temperature being lower than the pseudo-boiling temperature as mentioned above.

4 Conclusions

A pressure-based OF solver has been developed using the special algorithm proposed by Jarczyk et al. [7] to account for real-fluid effects. The descriptions of crucial steps in the implementation are provided. The developed solver has been used for simulations of transcritical and supercritical nitrogen jets injecting into warm surroundings. The numerical solutions obtained from the present work are in good agreement with the available experimental data of Mayer and coworkers [12]. It is verified that the results from this work are almost identical to those obtained from Muller et al. [8]. This implies the solver is successfully developed for real-fluid problems under transcritical and supercritical conditions. Future work will concentrate on the capabilities of the solver for reacting flows.

Acknowledgements

This work was supported by Basic Science Research Program through the National Research Foundation of Korea (NRF) funded by the Ministry of Science and ICT (NRF-2021R1A2C2005606).

References

- [1] The OpenFOAM Foundation Ltd. (2018). OpenFOAM: the open-source computational fluid dynamics (CFD) toolbox, version 6.
- [2] D. N. Nguyen, K. S. Jung, J. W. Shim, C. S. Yoo. (2022). Real-fluid thermophysicalModels: An OpenFOAM-based library for reacting flow simulations at high pressure. *Comput. Phys. Commun.* 273: 108264.
- [3] G. Soave. (1972). Equilibrium constants from a modified Redlich-Kwong equation of state. *Chem. Eng. Sci.* 27: 1197-1203.
- [4] M. S. Graboski, T. E. Daubert. (1978). A modified Soave equation of state for phase equilibrium calculations: 1. Hydrocarbon systems. *Ind. Eng. Chem. Process. Des. Dev.* 17: 443-448.
- [5] D. Peng, D. Robinson. (1976). A new two-constant equation of state. *Ind. Chem. Fundam.* 15: 59-64.
- [6] T. Chung, M. Ajlan, L. L. Lee, K. E. Starling. (1988). Generalized multiparameter correlation for nonpolar and polar fluid transport properties. *Ind. Eng. Chem. Res.* 27: 671-679.
- [7] M. Jarczyk, M. Pfitzner. (2012). Large Eddy simulation of supercritical nitrogen jets. 50th AIAA Aerospace Sciences Meeting. January 09-12, Nashville, Tennessee.
- [8] H. Muller, C. A. Neidermeier, M. Jarczyk, M. Pfitzner, S. Hickel, N. A. Adams. (2016). Large eddy simulation of trans- and supercritical injection. *Progress in Propulsion Physics* 8: 5-24.
- [9] C. Traxinger, J. Zips, M. Banholzer, M. Pfitzner. (2020). A pressure-based solution framework for sub- and supersonic flows considering real-gas effects and phase separation under engine-relevant conditions. *Comput. and Fluids* 202: 104452.
- [10] B. M. Ningegowda, F. N. Z. Rahantamialisoa, A. Pandal, H. Jasak, H. G. Im, M. Battistoni. (2020). Numerical modeling of transcritical and supercritical fuel injections using a multi-component two-phase flow model. *Energies* 13: 6576.
- [11] J. Hickey, P. Ma, M. Ihme. (2013). Large eddy simulation of shear coaxial rocket injector: real fluid effects. 49th AIAA/ASME/SAE/ASEE Joint Propulsion Conference. July 14-17, San Jose, CA.
- [12] W. Mayer, J. Telaar, R. Branam, G. schneider, J. Hussong. (2003). Raman measurements of cryogenic injection at supercritical pressure. *Heat and Mass Transfer* 39: 709-719.
- [13] J. Smagorinsky. (1963). General circulation experiments with the primitive equations. *Mon. Wea. Rev.* 91: 99-164.